

Melting heat transfer effects on stagnation point flow of micropolar fluid saturated in porous medium with internal heat generation (absorption)*

M. A. A. MAHMOUD¹, S. E. WAHEED^{1,2}

(1. Department of Mathematics, Faculty of Science, Benha University 13518, Benha, Egypt;

2. Department of Mathematics and Statistic, Faculty of Science,
Taif University 21974, Taif, Kingdom of Saudi Arabia)

Abstract The effect of melting heat transfer on the two dimensional boundary layer flow of a micropolar fluid near a stagnation point embedded in a porous medium in the presence of internal heat generation/absorption is investigated. The governing non-linear partial differential equations describing the problem are reduced to a system of non-linear ordinary differential equations using similarity transformations solved numerically using the Chebyshev spectral method. Numerical results for velocity, angular velocity and temperature profiles are shown graphically and discussed for different values of the inverse Darcy number, the heat generation/absorption parameter, and the melting parameter. The effects of the pertinent parameters on the local skin-friction coefficient, the wall couple stress, and the local Nusselt number are tabulated and discussed. The results show that the inverse Darcy number has the effect of enhancing both velocity and temperature and suppressing angular velocity. It is also found that the local skin-friction coefficient decreases, while the local Nusselt number increases as the melting parameter increases.

Key words melting effect, stagnation point, micropolar fluid, porous medium, heat generation (absorption)

Chinese Library Classification O361

2010 Mathematics Subject Classification 76A05, 76D10, 65S05

Nomenclature

c_p ,	specific heat at constant pressure;	M ,	melting parameter;
c_s ,	heat capacity of solid surface;	M_x ,	dimensionless wall couple stress;
C_{f_x} ,	local skin-friction coefficient;	m_0 ,	boundary parameter;
D_a^{-1} ,	permeability parameter;	m_w ,	wall couple stress;
f' ,	dimensionless velocity;	N ,	dimensional component of microrotation vector normal to x - y plane;
G ,	micro-rotation parameter;	Nu_x ,	local Nusselt number;
G_1 ,	micro-rotation constant;	Pr ,	Prandtl number;
h ,	dimensionless microrotation;	Q_0 ,	heat generation or absorption constant;
k ,	gyro-viscosity;	q_w ,	heat transfer from plate;
K ,	material parameter;	Re_x ,	local Reynolds number;
k_1 ,	permeability;		

* Received Oct. 8, 2013 / Revised Jan. 20, 2014

Corresponding author S. E. WAHEED, Ph. D., E-mail: shimaa_ezat@yahoo.com

T ,	fluid temperature;	T_m ,	temperature of melting surface;
T_0 ,	solid temperature;	T_∞ ,	free stream condition;
u, v ,	dimensional components of velocities along and perpendicular to plate, respec- tively;	x, y ,	dimensional distances along and perpen- dicular to plate, respectively.

Greek symbols

α ,	thermal diffusivity;	λ ,	latent heat fluid;
γ ,	heat generation or absorption param- eter;	μ ,	dynamic viscosity;
θ ,	dimensionless temperature;	ρ ,	fluid density;
κ ,	thermal conductivity;	τ_w ,	surface shear stress.

Subscripts

\prime , differentiation with respect to η .

1 Introduction

The structure of the flow near a stagnation-point is a fundamental topic in fluid dynamics, and it has attracted the attention of many researchers during the past several decades because of its wide industrial and technical applications, such as heat exchangers placed in a low-velocity environment, cooling of nuclear reactors during emergency shutdown, solar central receivers exposed to wind currents, cooling of electronic devices by fans, and many hydrodynamic processes. Hiemenz^[1] and Homann^[2] initiated the study of two dimensional and axisymmetric three dimensional stagnation point flows, respectively. Eckert^[3] extended Hiemenz's work by including the energy equation and obtained an exact similarity solution for the thermal field. Later, the problem of stagnation point flow was extended numerically by Schlichting and Bussmann^[4] and analytically by Ariel^[5] to include the effect of suction.

In recent years, the dynamics of micropolar fluids has become a popular area of research. The analysis of physical problems in these fluids has revealed several interesting phenomena, which are not found in Newtonian fluids, such as the extrusion of polymer fluids, solidification of liquid crystals, cooling of a metallic plate in a bath, animal bloods, fluids with additives, exotic lubricants, and colloidal, suspension solutions, and many other situations. Eringen^[6-7] was the first to propose the theory of micropolar fluids, in which the microscopic effects arising from the local structure and micromotions of the fluid elements are taken into account. Extensive reviews of this theory and its applications can be found in Refs. [8] and [9].

Many attempts were made to find analytical and numerical solutions by applying certain special conditions and using different mathematical approaches. Willson^[10] used the Karman-Polhausen approximate integral method to study the micropolar boundary-layer flow near a stagnation point. Peddieson and McNitt^[11] numerically studied the boundary-layer flow at a stagnation point under steady-state conditions using a finite difference scheme. A set of boundary layer equations for two dimensional flow of an incompressible micropolar fluid near a stagnation point was done by Bhargava and Rani^[12]. Ramachandran and Mathur^[13] studied the heat transfer in the stagnation point flow of a micropolar fluid. Heat transfer from non-isothermal surfaces in the stagnation-point flow of a micropolar fluid was studied by Unsworth and Chiam^[14]. Nazar et al.^[15] analyzed the steady stagnation flow towards a permeable vertical surface immersed in a micropolar fluid.

The porous media heat transfer problems have numerous thermal engineering applications such as geothermal energy recovery, crude oil extraction, thermal insulation, ground water pollution, thermal energy storage, and flow through filtering devices. Extensive reviews on this topic were provided in most recent books^[16-18]. Recently, Gupta and Sharma^[19] studied

the thermal instability of a micropolar fluid through a porous medium that has a constant thickness. The steady boundary layer flow of a micropolar fluid through a porous medium by using the generalized Darcys law was examined by Raptis^[20].

The melting process is encountered in a wide range of technologies, such as metal casting, laser manufacturing (drilling, welding, and selective sintering), seasonal freezing and melting of soil, lakes and rivers, and thermal energy storage. Epstein and Cho^[21] studied melting heat transfer from a flat plate in a steady laminar case, while Kazmierczak et al.^[22–23] considered melting from a vertical flat plate embedded in a porous medium in both natural and forced convection modes.

Cheng and Lin^[24–25] examined melting effect on mixed convective heat transfer from a porous vertical plate in a liquid-saturated porous medium with aiding and opposing external flows. Carslaw and Jaeger^[26] discussed melting of a semi-infinite body with constant thermo-physical properties and obtained an analytical solution for Dirichlet boundary conditions. Raisi and Rostami^[27] investigated numerically the temperature distribution and melt pool size in a semi-infinite body due to a moving Laser heat source. Kearns and Plumb^[28] experimentally studied direct contact melting of a packed bed. The magnetic and buoyancy effects on melting processes about a vertical wall embedded in a saturated porous medium were investigated by Tashtoush^[29]. Very recently, Ishak et al.^[30] studied the steady laminar boundary layer flow and heat transfer from a warm, laminar liquid flow to a melting surface moving parallel to a constant free stream. Moreover, the melting heat transfer in boundary layer stagnation-point flow towards a stretching (shrinking) sheet problem was studied by Bachok et al.^[31].

Motivated by all these works, we contemplate to study the melting effects on flow and heat transfer of a micropolar fluid near stagnation point embedded in a porous medium in the presence of internal heat generation (absorption).

2 Formulation of problem

Consider stagnation point flow of an incompressible micropolar fluid towards a horizontal plate embedded in a porous medium. It is assumed that the plate constitutes the interface between the liquid phase and the solid phase during melting inside the porous matrix at the steady state. The coordinate system and flow model are shown in Fig. 1. The x -axis is directed along the plate and the y -axis is normal to it. It is assumed that the velocity of the external flow is $U(x) = ax$, where a is a positive constant, and x measures the distance from the leading edge along the surface of the plate. The plate is at constant temperature T_m at which the material of the porous matrix melts (the liquid phase temperature is $T_\infty (> T_m)$ and the temperature of the solid far from the interface is $T_0 (< T_m)$). The flow is steady, laminar, and two-dimensional.

Under the usual boundary-layer approximations, the basic equations taking into account the presence of internal heat generation (absorption) in the energy equation for a micropolar fluid can be written as follows^[32]:

$$\frac{\partial u}{\partial x} + \frac{\partial v}{\partial y} = 0, \quad (1)$$

$$u \frac{\partial u}{\partial x} + v \frac{\partial u}{\partial y} = U \frac{dU}{dx} + \left(\frac{\mu + k}{\rho} \right) \frac{\partial^2 u}{\partial y^2} + \frac{k}{\rho} \frac{\partial N}{\partial y} - \frac{\mu}{\rho k_1} (u - U), \quad (2)$$

$$G_1 \frac{\partial^2 N}{\partial y^2} - \left(2N + \frac{\partial u}{\partial y} \right) = 0, \quad (3)$$

$$u \frac{\partial T}{\partial x} + v \frac{\partial T}{\partial y} = \alpha \frac{\partial^2 T}{\partial y^2} + \frac{q'''}{\rho c_p}, \quad (4)$$

where u and v are the velocity components in the x - and y -directions, respectively. N is the

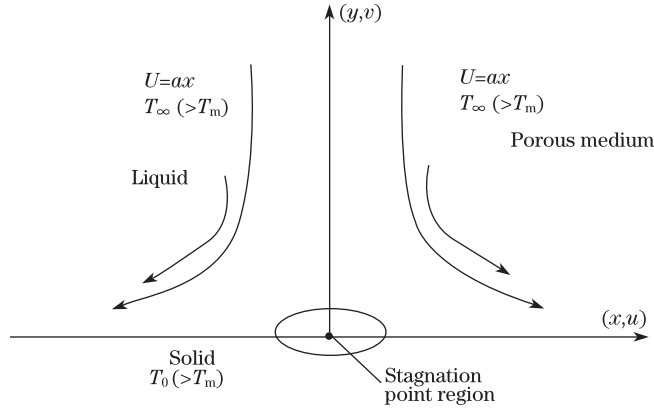


Fig. 1 Flow model and coordinate system

component of the micro-rotation vector normal to the xy -plane, T is the fluid temperature, μ is the dynamic viscosity, k is the gyro-viscosity (or vortex viscosity), ρ is the fluid density, k_1 is the permeability of the porous medium, $G_1 = \frac{\gamma^*}{k}$ is the microrotation constant, α is the thermal diffusivity of the fluid, and c_p is the specific heat at constant pressure.

Following Epstein and Cho^[21], we assume that the boundary conditions are as follows:

$$\begin{cases} u = 0, & N = -m_0 \frac{\partial u}{\partial y}, & T = T_m & \text{at } y = 0, \\ u \rightarrow U(x), & N \rightarrow 0, & T \rightarrow T_\infty & \text{as } y \rightarrow \infty, \end{cases} \quad (5)$$

and

$$\kappa \left(\frac{\partial T}{\partial y} \right)_{y=0} = \rho(\lambda + c_s(T_m - T_0))v(x, 0), \quad (6)$$

where m_0 ($0 \leq m_0 \leq 1$) is the boundary parameter. When the boundary parameter $m_0 = 0$, we obtain $N = 0$ which is the no-spin condition, i.e., the microelements in a concentrated particle flow close to the wall are not able to rotate (as stipulated by Jena and Mathur^[33]). The case $m_0 = 1/2$, represents the weak concentration of microelements. The case corresponding to $m_0 = 1$ is used for the modelling of turbulent boundary layer flow (see Peddison and McNitt^[11]). In (6), κ is the thermal conductivity, λ is the latent heat fluid, and c_s is the heat capacity of the solid surface. (6) states that the heat conducted to the melting surface is equal to the heat of melting plus the sensible heat required to raise the solid temperature T_0 to its melting temperature T_m (see Epstein and Cho^[21] and Bachok et al.^[31]). In order to get a similarity solution, the dependence of the internal heat generation (absorption) rate of the space coordinate can be taken in the form^[34]:

$$q''' = Q_0 e^{-\eta}, \quad (7)$$

where Q_0 is the heat generation or absorption constant.

We introduce the following dimensionless variables:

$$\begin{cases} \eta = \left(\frac{a}{\nu} \right)^{1/2} y, & N = ax \left(\frac{a}{\nu} \right)^{1/2} h(\eta), \\ u = ax f'(\eta), & v = -(a\nu)^{1/2} f, \\ \theta(\eta) = \frac{T - T_m}{T_\infty - T_m}. \end{cases} \quad (8)$$

Through (8), the continuity equation (1) is automatically satisfied. From (2)–(4), we can get

$$(1 + K)f''' + ff'' - f'^2 + Kh' + D_a^{-1}(1 - f') + 1 = 0, \quad (9)$$

$$Gh'' - (2h + f'') = 0, \quad (10)$$

$$\frac{1}{Pr}\theta'' + f\theta' + \gamma e^{-\eta} = 0. \quad (11)$$

The transformed boundary conditions are then given as follows:

$$\begin{cases} f' = 0, & Prf + M\theta' = 0, \\ h = -m_0f'', & \theta = 0 \quad \text{at} \quad \eta = 0, \\ f' \rightarrow 1, & h \rightarrow 0, \quad \theta \rightarrow 1 \quad \text{as} \quad \eta \rightarrow \infty, \end{cases} \quad (12)$$

where primes denote differentiation with respect to η ,

$$K = \frac{k}{\mu}, \quad D_a^{-1} = \frac{\nu}{ak_1}, \quad G = G_1a/\nu, \\ Pr = \mu c_p/\kappa, \quad \gamma = \frac{Q_0}{a\rho c_p(T_\infty - T_m)}.$$

Here, γ is the heat generation ($\gamma > 0$) or absorption ($\gamma < 0$) parameter, and M is the dimensionless melting parameter which is defined as

$$M = \frac{c_p(T_\infty - T_m)}{\lambda + c_s(T_m - T_0)}. \quad (13)$$

The melting parameter is a combination of the two Stefan numbers $c_f(T_\infty - T_m)/\lambda$ and $c_s(T_m - T_0)/\lambda$ for the liquid and solid phases, respectively.

The physical quantities of interest are the local skin-friction coefficient C_{f_x} , the dimensionless wall couple stress M_x and the local Nusselt number Nu_x , which are defined as follows:

$$\begin{cases} C_{f_x} = \frac{2\tau_w}{\rho U^2}, \\ M_x = \frac{m_w}{\rho a \nu U(x)x^2}, \\ Nu_x = \frac{xq_w}{\kappa(T_\infty - T_m)}, \end{cases} \quad (14)$$

where the surface shear stress τ_w , the wall couple stress m_w , and the heat transfer from the plate q_w are defined by

$$\begin{cases} \tau_w = \left((\mu + K) \frac{\partial u}{\partial y} + KN \right)_{y=0}, \\ m_w = \gamma^* \left(\frac{\partial N}{\partial y} \right)_{y=0}, \\ q_w = - \left(\kappa \frac{\partial T}{\partial y} \right)_{y=0}. \end{cases} \quad (15)$$

Using the similarity variables (13), we get

$$\begin{cases} \frac{1}{2}C_{f_x}Re_x^{1/2} = (1 + K(1 - m_0))f''(0), \\ M_xRe_x = KGh'(0), \\ Nu_xRe_x^{-1/2} = -\theta'(0), \end{cases} \quad (16)$$

where $Re_x (= \frac{U(x)x}{\nu})$ is the local Reynolds number.

3 Method of solution

The governing boundary layer equations (9)–(12) have the domain $0 \leq \eta \leq \eta_\infty$, where η_∞ is one end of the user specified computational domain. Using the algebraic mapping

$$\chi = 2\frac{\eta}{\eta_\infty} - 1,$$

the unbounded region $[0, \infty)$ is mapped into the finite domain $[1, -1]$, and the problem expressed by equations (9)–(12) is transformed to the following system:

$$\begin{aligned} (1 + K)f'''(\chi) + \left(\frac{\eta_\infty}{2}\right)(f(\chi)f''(\chi) - f'^2(\chi)) \\ + \left(\frac{\eta_\infty}{2}\right)^2 \left(Kh'(\chi) - D_a^{-1}\left(\left(\frac{\eta_\infty}{2}\right) - f'(\chi)\right)\right) + \left(\frac{\eta_\infty}{2}\right)^3 = 0, \end{aligned} \quad (17)$$

$$Gh''(\chi) - \left(2\left(\frac{\eta_\infty}{2}\right)^2 h(\chi) + f''(\chi)\right) = 0, \quad (18)$$

$$\frac{1}{Pr}\theta''(\chi) + \left(\frac{\eta_\infty}{2}\right)f(\chi)\theta'(\chi) + \left(\frac{\eta_\infty}{2}\right)^2 \gamma e^{-(\frac{\eta_\infty}{2})(1+\chi)} = 0. \quad (19)$$

The transformed boundary conditions are given as follows:

$$\begin{cases} Prf(-1) + M\left(\frac{2}{\eta_\infty}\right)\theta'(-1) = 0, \\ f'(-1) = 0, \quad f'(1) = \left(\frac{\eta_\infty}{2}\right), \\ h(-1) = -m_0\left(\frac{2}{\eta_\infty}\right)^2 f''(-1), \quad h(1) = 0, \\ \theta(-1) = 0, \quad \theta(1) = 1. \end{cases} \quad (20)$$

Our technique is accomplished by starting with a Chebyshev approximation for the highest order derivatives, f''' , h'' , and θ'' and generating approximations to the lower order derivatives f'' , f' , f , h' , h , θ' and θ as follows.

Setting

$$f''' = \phi(\chi), \quad h'' = \psi(\chi), \quad \theta'' = \zeta(\chi),$$

then by integration, we obtain

$$f''(\chi) = \int_{-1}^{\chi} \phi(\chi) d\chi + C_1^f, \quad (21)$$

$$f'(\chi) = \int_{-1}^{\chi} \int_{-1}^{\chi} \phi(\chi) d\chi d\chi + C_1^f(\chi + 1) + C_2^f, \quad (22)$$

$$f(\chi) = \int_{-1}^{\chi} \int_{-1}^{\chi} \int_{-1}^{\chi} \phi(\chi) d\chi d\chi d\chi + C_1^f \frac{(\chi + 1)^2}{2} + C_2^f(\chi + 1) + C_3^f, \quad (23)$$

$$h'(\chi) = \int_{-1}^{\chi} \psi(\chi) d\chi + C_1^h, \quad (24)$$

$$h(\chi) = \int_{-1}^{\chi} \int_{-1}^{\chi} \psi(\chi) d\chi d\chi + C_1^h(\chi + 1) + C_2^h, \quad (25)$$

$$\theta'(\chi) = \int_{-1}^{\chi} \zeta(\chi) d\chi + C_1^\theta, \quad (26)$$

$$\theta(\chi) = \int_{-1}^{\chi} \int_{-1}^{\chi} \zeta(\chi) d\chi d\chi + C_1^\theta(\chi + 1) + C_2^\theta. \quad (27)$$

From the boundary condition (20), we obtain

$$C_1^f = \frac{1}{2} \left(\frac{\eta_\infty}{2} \right) - \frac{1}{2} \int_{-1}^1 \int_{-1}^{\chi} \phi(\chi) d\chi d\chi,$$

$$C_2^f = 0,$$

$$C_3^f = \frac{M}{2Pr} \left(\frac{2}{\eta_\infty} \right) \int_{-1}^1 \int_{-1}^{\chi} \zeta(\chi) d\chi d\chi - \frac{M}{2Pr} \left(\frac{2}{\eta_\infty} \right),$$

$$C_1^h = -\frac{1}{2} \int_{-1}^1 \int_{-1}^{\chi} \psi(\chi) d\chi - \frac{1}{2} C_2^h,$$

$$C_2^h = \frac{m_0}{2} \left(\frac{2}{\eta_\infty} \right)^2 \int_{-1}^1 \int_{-1}^{\chi} \phi(\chi) d\chi d\chi - \frac{m_0}{2} \left(\frac{2}{\eta_\infty} \right),$$

$$C_1^\theta = -\frac{1}{2} \int_{-1}^1 \int_{-1}^{\chi} \zeta(\chi) d\chi d\chi + \frac{1}{2},$$

$$C_2^\theta = 0.$$

Therefore, we can give approximations to (21)–(27) as follows:

$$\begin{cases} f_i(\chi) = \sum_{j=0}^n l_{ij}^f \phi_j + d_i^f, \\ f'_i(\chi) = \sum_{j=0}^n l_{ij}^{f1} \phi_j + d_i^{f1}, \\ f''_i(\chi) = \sum_{j=0}^n l_{ij}^{f2} \phi_j + d_i^{f2}, \end{cases} \quad (28)$$

$$\begin{cases} h_i(\chi) = \sum_{j=0}^n l_{ij}^\theta \psi_j + \sum_{j=0}^n l_{ij}^h \phi_j + d_i^h, \\ h'_i(\chi) = \sum_{j=0}^n l_{ij}^{\theta 1} \psi_j + \sum_{j=0}^n l_{ij}^{h 1} \phi_j + d_i^{h 1}, \end{cases} \tag{29}$$

$$\begin{cases} \theta_i(\chi) = \sum_{j=0}^n l_{ij}^\theta \zeta_j + d_i^\theta, \\ \theta'_i(\chi) = \sum_{j=0}^n l_{ij}^{\theta 1} \zeta_j + d_i^{\theta 1} \end{cases} \tag{30}$$

for all $i = 0, \dots, n$, where

$$\begin{aligned} l_{ij}^\theta &= b_{ij}^2 - \frac{(\chi_i + 1)}{2} b_{nj}^2, & d_i^\theta &= \frac{(\chi_i + 1)}{2}, \\ l_{ij}^{\theta 1} &= b_{ij} - \frac{1}{2} b_{nj}^2, & d_i^{\theta 1} &= \frac{1}{2}, \\ l_{ij}^h &= \frac{m_0}{2} \left(\frac{2}{\eta_\infty}\right)^2 \left(1 - \frac{(\chi_i + 1)}{2}\right) b_{nj}^2, & d_i^h &= \frac{m_0}{2} \left(\frac{2}{\eta_\infty}\right) \left(\frac{(\chi_i + 1)}{2} - 1\right), \\ l_{ij}^{h 1} &= -\frac{m_0}{4} \left(\frac{2}{\eta_\infty}\right)^2 b_{nj}^2, & d_i^{h 1} &= \frac{m_0}{4} \left(\frac{2}{\eta_\infty}\right), \\ l_{ij}^f &= b_{ij}^3 - \frac{(\chi_i + 1)^2}{4} b_{nj}^2, & \bar{l}_{ij}^f &= \frac{M}{2Pr} \left(\frac{2}{\eta_\infty}\right) b_{nj}^2, & d_i^f &= \frac{(\chi_i + 1)^2}{4} \left(\frac{\eta_\infty}{2}\right) - \frac{M}{2Pr} \left(\frac{2}{\eta_\infty}\right), \\ l_{ij}^{f 1} &= b_{ij}^2 - \frac{(\chi_i + 1)}{2} b_{nj}^2, & \bar{l}_{ij}^{f 1} &= 0, & d_i^{f 1} &= \frac{(\chi_i + 1)}{2} \left(\frac{\eta_\infty}{2}\right), \\ l_{ij}^{f 2} &= b_{ij} - \frac{1}{2} b_{nj}^2, & \bar{l}_{ij}^{f 2} &= 0, & d_i^{f 2} &= \frac{1}{2} \left(\frac{\eta_\infty}{2}\right), \end{aligned}$$

where $\chi_i = -\cos(\frac{i\pi}{n})$ are the Chebyshev points.

$$b_{ij}^2 = (\chi_i - \chi_j) b_{ij},$$

and b_{ij} are the elements of the matrix B , as given in Ref. [35].

By using (28)–(30), one can transform (17)–(19) to the following system of nonlinear equations in the highest derivatives into the following Chebyshev spectral equations:

$$\begin{aligned} (1 + K)\phi_i + \left(\frac{\eta_\infty}{2}\right) &\left(\left(\sum_{j=0}^n l_{ij}^f \phi_j + \sum_{j=0}^n \bar{l}_{ij}^f \zeta_j + d_i^f\right) \left(\sum_{j=0}^n l_{ij}^{f 2} \phi_j + \sum_{j=0}^n \bar{l}_{ij}^{f 2} \zeta_j + d_i^{f 2}\right)\right. \\ &- \left.\left(\sum_{j=0}^n l_{ij}^{f 1} \phi_j + \sum_{j=0}^n \bar{l}_{ij}^{f 1} \zeta_j + d_i^{f 1}\right)^2\right) + \left(\frac{\eta_\infty}{2}\right)^2 \left(K \left(\sum_{j=0}^n l_{ij}^{\theta 1} \psi_j + \sum_{j=0}^n l_{ij}^{h 1} \phi_j + d_i^{h 1}\right)\right. \\ &+ \left. D_a^{-1} \left(\left(\frac{\eta_\infty}{2}\right) - \left(\sum_{j=0}^n l_{ij}^{f 1} \phi_j + \sum_{j=0}^n \bar{l}_{ij}^{f 1} \zeta_j + d_i^{f 1}\right)\right)\right) + \left(\frac{\eta_\infty}{2}\right)^3 = 0, \end{aligned} \tag{31}$$

$$G\psi_i - \left(2\left(\frac{\eta_\infty}{2}\right)^2 \left(\sum_{j=0}^n l_{ij}^\theta \psi_j + \sum_{j=0}^n l_{ij}^h \phi_j + d_i^h\right) + \left(\sum_{j=0}^n l_{ij}^{f 2} \phi_j + \sum_{j=0}^n \bar{l}_{ij}^{f 2} \zeta_j + d_i^{f 2}\right)\right) = 0, \tag{32}$$

$$\begin{aligned} \frac{1}{Pr} \zeta_i + \left(\frac{\eta_\infty}{2}\right) &\left(\sum_{j=0}^n l_{ij}^f \phi_j + \sum_{j=0}^n \bar{l}_{ij}^f \zeta_j + d_i^f\right) \left(\sum_{j=0}^n l_{ij}^{\theta 1} \zeta_j + d_i^{\theta 1}\right) \\ &+ \left(\frac{\eta_\infty}{2}\right)^2 \gamma e^{-(\frac{\eta_\infty}{2})(1+\chi_i)} = 0. \end{aligned} \tag{33}$$

This system is then solved using Newton's iteration method with $n = 11$; the computer program is executed in Mathematica 4 running on a PC.

4 Results and discussion

In order to assess the accuracy of the present numerical method, we compare our numerical results obtained for $f''(0)$ with those reported by Hiemenz^[1] and Bachok et al.^[31] and for $\theta'(0)$ with those reported by Yacob et al.^[36] for parameters, $K = 0$, $D_a^{-1} = 0$, and $\gamma = 0$ in (9) and (11), and for various values of M . The results show a good agreements, as seen in Table 1 and Table 2.

The effects of the various parameters such as the inverse Darcy number, the melting parameter, and the heat generation (absorption) parameter on the velocity, the angular velocity, and the temperature profiles are shown in Figs. 2–10.

Table 1 Comparison between present numerical results and results given by Hiemenz^[1] and Bachok et al.^[31] of $f''(0)$ for various values of M with $K = 0$, $D_a^{-1} = 0$, and $\gamma = 0$

M	Hiemenz ^[1]	Bachok et al. ^[31]	Present work
0	1.232 600	1.232 587	1.232 600
1	–	1.037 003	1.036 997
2	–	0.946 850	0.946 849
3	–	0.891 381	0.891 363

Table 2 Comparison between present numerical results and results given by Yacob et al.^[36] of $\theta'(0)$ for various values of M with $K = 0$, $D_a^{-1} = 0$, and $\gamma = 0$

M	Yacob et al. ^[36]	Present work
0	0.570 465	0.570 464 5
1	0.361 961	0.361 960 9

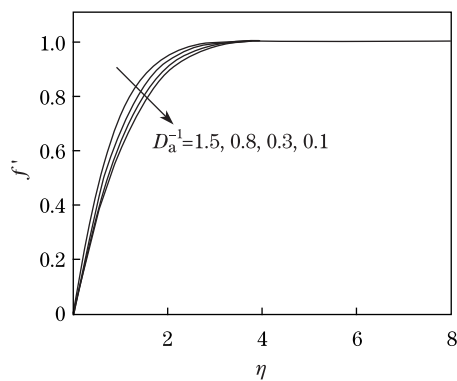


Fig. 2 Velocity profiles for various values of D_a^{-1} with $G = 2$, $K = 1.2$, $Pr = 1$, $m_0 = 0.5$, and $Q = 0.1$

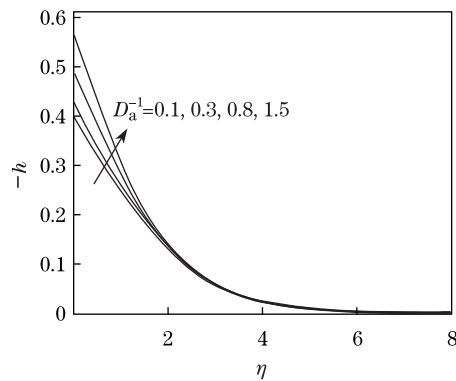


Fig. 3 Angular velocity profiles for various values of D_a^{-1} with $G = 2$, $K = 1.2$, $M = 2$, $Pr = 1$, $m_0 = 0.5$, and $Q = 0.1$

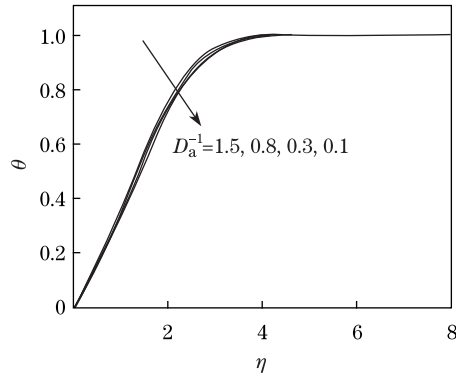


Fig. 4 Temperature profiles for various values of D_a^{-1} with $G = 2$, $K = 1.2$, $M = 2$, $Pr = 1$, $m_0 = 0.5$, and $Q = 0.1$

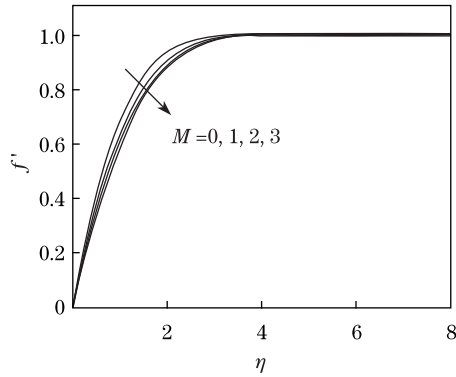


Fig. 5 Velocity profiles for various values of M with $G = 2$, $K = 1.2$, $D_a^{-1} = 0.1$, $Pr = 1$, $m_0 = 0.5$, and $Q = 0.1$

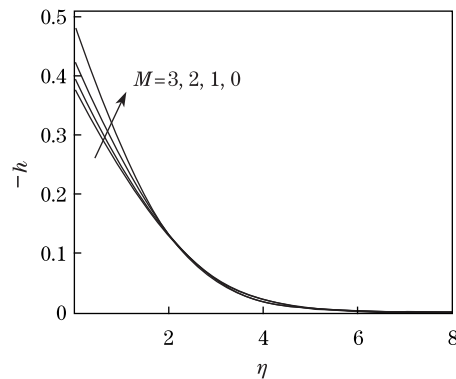


Fig. 6 Angular velocity profiles for various values of M with $G = 2$, $K = 1.2$, $D_a^{-1} = 0.1$, $Pr = 1$, $m_0 = 0.5$, and $Q = 0.1$

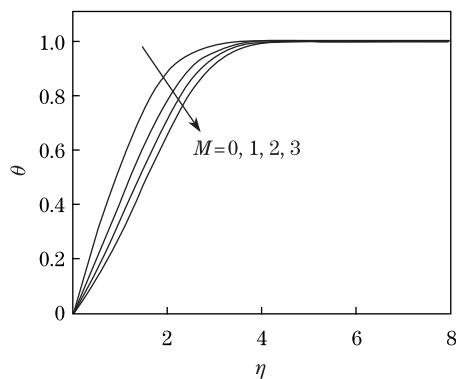


Fig. 7 Temperature profiles for various values of M with $G = 2$, $K = 1.2$, $D_a^{-1} = 0.1$, $Pr = 1$, $m_0 = 0.5$, and $Q = 0.1$

Figure 2 presents the effect of the inverse Darcy number D_a^{-1} on f' . We notice that f' increases with the increase of D_a^{-1} . This is due to increasing the inverse Darcy number means an increase of the porosity of the medium. For increasing porosity, the space allowing fluid to move in a porous medium becomes large. Consequently, the fluid velocity increases. Figure 3 displays the influence of D_a^{-1} on the angular velocity. It is obvious that initially h decreases by increasing D_a^{-1} near the surface and the reverse is true away from the surface. It is noticed that large values of D_a correspond to high porosity of the porous medium, and the limit $D_a \rightarrow \infty$ corresponds to the case of absence of the porous medium. The presence of porous medium causes higher retardation to the fluid, which reduces the velocity. Figure 4 illustrates the effects of D_a^{-1} on the temperature profiles θ . It is observed that θ increases with the increase of D_a^{-1} . Figure 5 shows the variation of $f'(\eta)$ with η for various values of the melting parameter M . It can be seen that f' decreases with the increase of M . This is in agreement with the fact that more intense melting (increasing M) tends to thicken the boundary layer. The angular velocity profiles for different values of M are illustrated in Fig. 6, which shows that h increases with the increase of M near the surface and the reverse is true at large distances from the surface. It

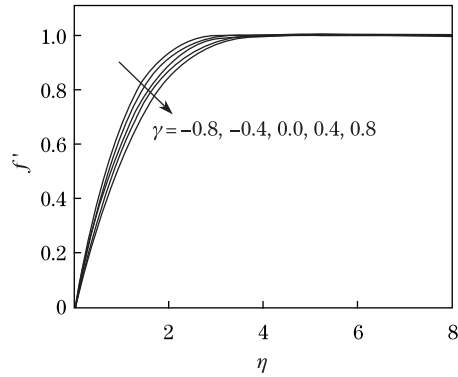


Fig. 8 Velocity profiles for various values of γ with $G = 2$, $K = 1.2$, $D_a^{-1} = 0.1$, $Pr = 1$, $m_0 = 0.5$, and $M = 2$

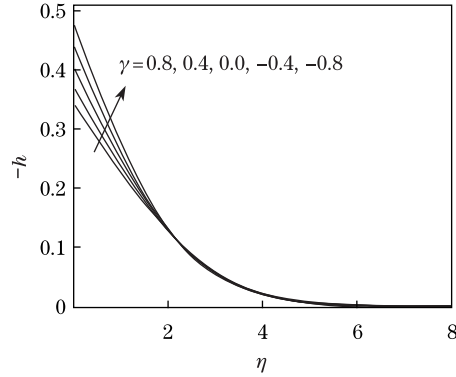


Fig. 9 Angular velocity profiles for various values of γ with $G = 2$, $K = 1.2$, $D_a^{-1} = 0.1$, $Pr = 1$, $m_0 = 0.5$, and $M = 2$

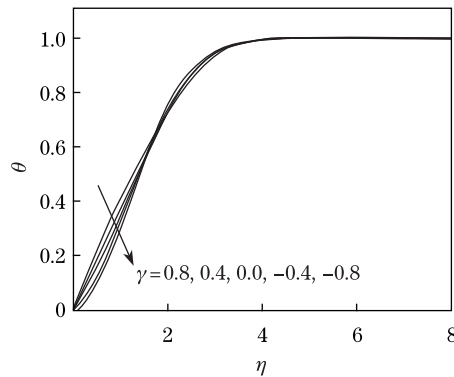


Fig. 10 Temperature profiles for various values of γ with $G = 2$, $K = 1.2$, $D_a^{-1} = 0.1$, $Pr = 1$, $m_0 = 0.5$, and $M = 2$

can be noticed that the temperature profiles decrease as M increases as illustrated in Fig. 7. Physically, increasing the melting parameter causes higher acceleration to the fluid flow which, in turn, increases its motion and causes decrease in the temperature profiles. The effects of the heat generation parameter ($\gamma > 0$) and the absorption parameter ($\gamma < 0$) on the velocity, the angular velocity and the temperature are displayed in Figs. 8, 9, and 10, respectively. It is seen from Fig. 8 that f' decreases as the heat generation parameter ($\gamma > 0$) increases, but the effect of the absolute value of the heat absorption parameter ($\gamma < 0$) is opposite. In Fig. 9, it is shown that h increases as the heat generation parameter increases, while h decreases as the absolute value of the heat absorption parameter increases near the surface and the opposite is true away from it. Figure 10 displays the effect of the heat generation (absorption) parameter on the temperature profiles θ . It is found that as the heat generation parameter increases θ increases near the surface and the reverse is true away from the surface, while the effect of the absolute value of the absorption parameter is opposite.

Table 3 illustrates the effects of D_a^{-1} , M , and γ on the local skin-friction coefficient in terms of $f''(0)$, the dimensionless wall couple stress in terms of $h'(0)$, and the local Nusselt number in terms of $-\theta'(0)$. From this Table, it is observed that the local skin-friction coefficient and the dimensionless wall couple stress increase with increasing D_a^{-1} , but the local Nusselt number decreases with increasing D_a^{-1} . Moreover, it is also found that, increasing M leads to

a decrease in the local skin-friction coefficient and the dimensionless wall couple stress, while the local Nusselt number increases as M increases. This is because increasing the melting parameter M increases the thermal boundary layer thickness which results in a reduction in temperature gradient at the surface. Finally, we can see that the local skin-friction coefficient, the dimensionless wall couple stress and the local Nusselt number decrease with increasing the heat generation parameter, but the reverse is true for the absolute values of the heat absorption parameter.

Table 3 Values of $f''(0)$, $h'(0)$, and $\theta'(0)$ with $m_0 = 0.5$, $K = 1.2$, $G = 2$, and $Pr = 1$

D_a^{-1}	M	γ	$f''(0)$	$h'(0)$	$\theta'(0)$
0.1	2	0.1	0.794 517	0.155 405	0.293 257
0.3	2	0.1	0.849 944	0.175 904	0.296 545
0.8	2	0.1	0.975 463	0.223 595	0.303 364
1.5	2	0.1	1.128 810	0.283 946	0.310 690
0.1	0	0.1	0.971 549	0.219 799	0.604 407
0.1	1	0.1	0.852 142	0.175 850	0.385 372
0.1	2	0.1	0.794 517	0.155 405	0.293 257
0.1	3	0.1	0.757 662	0.142 633	0.240 549
0.1	2	0.8	0.688 602	0.119 424	0.495 754
0.1	2	0.4	0.746 486	0.138 810	0.381 880
0.1	2	0	0.811 384	0.161 332	0.263 217
0.1	2	-0.4	0.882 944	0.186 995	0.141 137
0.1	2	-0.8	0.960 621	0.215 698	0.016 891

5 Conclusions

The problem of steady two-dimensional flow of a micropolar fluid at stagnation point embedded in a porous medium with melting heat transfer and in the presence of internal heat generation (absorption) has been investigated. Using similarity transformations, the governing equations are transformed into a system of coupled non-linear ordinary differential equations which is solved numerically by using the Chebyshev spectral method. The results show that the numerical values of the local skin-friction coefficient and the dimensionless wall couple stress increase as the inverse Darcy number increases, while it decreases as the melting parameter increases. The local Nusselt number decreases with increasing the inverse Darcy number, while the melting parameter leads to an increase in the local Nusselt number. Also, it can be found that the local skin-friction coefficient, the dimensionless wall couple stress and the local Nusselt number decrease with increasing of the heat generation parameter, but the opposite is true for the absolute values of the heat absorption parameter.

Acknowledgements The authors would like to thank the reviewers for their valuable comments, which lead to the improvement of the work.

References

- [1] Hiemenz, K. Die Grenzschicht an einem in den gleichförmigen Flüssigkeitsstrom eingetauchten geraden Kreiszylinder. *Dinglers Polytechnisches Journal*, **326**, 321–410 (1911)
- [2] Homann, F. Der Einfluss grosser Zähigkeit bei der Strömung um den Zylinder und um die Kugel. *Zeitschrift für Angewandte Mathematik und Mechanik*, **16**, 153–165 (1936)
- [3] Eckert, E. R. G. *VDI Forschungsheft*, Berlin, 416–418 (1942)
- [4] Schlichting, H. and Busmann, K. Exakte Lösungen für die laminare Reibungsschicht mit Absaugung und Ausblasen. *Schriften Deutschen Akademie der Luftfahrtforschung Series B*, **7**, 25–69 (1943)

-
- [5] Ariel, P. D. Stagnation point flow with suction: an approximate solution. *Journal of Applied Mechanics*, **61**, 976–978 (1994)
- [6] Eringen, A. Theory of micropolar fluids. *Journal of Applied Mathematics and Mechanics*, **16**, 1–18 (1966)
- [7] Eringen, A. Theory of thermomicrofluids. *Journal of Mathematical Analysis and Applications*, **9**, 480–496 (1972)
- [8] Armin, T., Turk, M. A., and Sylvester, N. D. Microcontinuum fluid mechanics a review. *International Journal of Engineering Science*, **11**, 905–915 (1973)
- [9] Armin, T., Turk, M. A., and Sylvester, N. D. Application of microcontinuum fluid mechanics. *International Journal of Engineering Science*, **12**, 273–279 (1974)
- [10] Willson, A. J. Boundary layers in micropolar liquids. *Proceedings of the Cambridge Philosophical Society*, **67**, 46–57 (1970)
- [11] Peddieson, J. and McNitt, R. P. Boundary-layer theory for a micropolar fluid. *Recent Advances in Engineering Science*, **5**, 405–426 (1970)
- [12] Bhargava, R. and Rani, M. Heat transfer in micropolar boundary layer flow near a stagnation point. *International Journal of Engineering Science*, **23**, 1331–1335 (1985)
- [13] Ramachandran, P. S. and Mathur, M. N. Heat transfer in the stagnation point flow of a micropolar fluid. *Acta Mechanica*, **36**, 247–261 (1980)
- [14] Unsworth, K. and Chiam, T. C. Heat transfer from non-isothermal surfaces in the stagnation-point flow of a micropolar fluid. *Rheologica Acta*, **19**, 356–364 (1980)
- [15] Nazar, R., Ishak, A., and Pop, I. Stagnation flow of a micropolar fluid towards a vertical permeable surface. *International Communications in Heat and Mass Transfer*, **35**, 276–281 (2008)
- [16] Ingham, D. B. and Pop, I. *Transport Phenomena in Porous Media*, Pergamon, Oxford (1998)
- [17] Vafai, K. *Handbook of Porous Media*, Taylor and Francis, Baton Rouge (2005)
- [18] Nield, D. A. and Bejan, A. *Convection in Porous Media*, Springer, New York (2006)
- [19] Gupta, U. and Sharma, R. S. Thermal convection in micropolar fluids in porous medium. *International Journal of Engineering Science*, **33**, 1887–1892 (1995)
- [20] Raptis, A. Boundary layer flow of a micropolar fluid through a porous medium. *Journal of Porous Media*, **3**, 95–96 (2000)
- [21] Epstein, M. and Cho, D. H. Melting heat transfer in steady laminar flow over a flat plate. *Journal of Heat Transfer*, **98**, 531–533 (1976)
- [22] Kazmierczak, M., Poulikakos, D., and Sadowski, D. Melting of a vertical plate in porous medium controlled by forced convection of a dissimilar fluid. *International Communications in Heat and Mass Transfer*, **14**, 507–517 (1987)
- [23] Kazmierczak, M., Poulikakos, D., and Pop, I. Melting from a flat plate in a porous medium in the presence of steady natural convection. *Numerical Heat Transfer*, **10**, 571–581 (1986)
- [24] Cheng, W. T. and Lin, C. H. Transient mixed convective heat transfer with melting effect from the vertical plate in a liquid saturated porous medium. *International Journal of Engineering Science*, **44**, 1023–1036 (2006)
- [25] Cheng, W. T. and Lin, C. H. Melting effect on mixed convective heat transfer with aiding and opposing external flows from the vertical plate in a liquid saturated porous medium. *International Journal of Heat and Mass Transfer*, **50**, 3026–3034 (2007)
- [26] Carslaw, H. S. and Jaeger, J. C. *Conduction of Heat in Solids*, Clarendon Press, Oxford (2006)
- [27] Raisi, A. and Rostami, A. A. Temperature distribution and melt pool size in a semi-infinite body due to a moving laser heat source. *Numerical Heat Transfer Part A*, **31**, 783–796 (1997)
- [28] Kearns, D. A. and Plumb, O. A. Direct contact melting of a packed bed. *Journal of Heat Transfer*, **150**, 452–457 (1995)
- [29] Tashtoush, B. Magnetic and buoyancy effects on melting from a vertical plate embedded in saturated porous media. *Energy Conversion and Management*, **46**, 2566–2577 (2005)
- [30] Ishak, A., Nazar, R., Bachok, N., and Pop, I. Melting heat transfer in steady laminar flow over a moving surface. *Heat Mass Transfer*, **46**, 463–468 (2010)

- [31] Bachok, N., Ishak, A., and Pop, I. Melting heat transfer in boundary layer stagnation-point flow towards a stretching/shrinking sheet. *Physics Letters A*, **374**, 4075–4079 (2010)
- [32] Takhar, H. S. and Soundalgekar, V. M. Flow of a micropolar fluid on a continuous moving plate. *International Journal of Engineering Science*, **21**, 961–965 (1983)
- [33] Jena, S. K. and Mathur, M. N. Similarity solution for laminar free convection flow of thermo-micropolar fluid past a non-isothermal vertical flat plate. *International Journal of Engineering Science*, **19**, 1431–1439 (1981)
- [34] Crepeau, R. V. and Clarksean, R. Similarity solutions of natural convection with internal heat generation. *Journal of Heat Transfer*, **119**, 183–185 (1997)
- [35] El-Gendi, S. E. Chebyshev solution of differential, integral and integro-differential equations. *Computer Journal*, **12**, 282–287 (1969)
- [36] Yacob, N. A., Ishak, A., and Pop, I. Melting heat transfer in boundary layer stagnation point flow towards a stretching/shrinking sheet in a micropolar fluid. *Computer & Fluids*, **47**, 16–21 (2011)